Available online at www.sciencedirect.com
ScienceDirect
International Journal of Heat and Mass Transfer 51 (2008) 2801–2813
International Journal of HEAT and MASS TRANSFER
www.elsevier.com/locate/ijhmt

Studies on gas–solid heat transfer during pneumatic conveying

K.S. Rajan [a,*], K. Dhasandhan [a], S.N. Srivastava [a], B. Pitchumani [b]

[a] School of Chemical and Biotechnology, SASTRA University, Tirumalaisamudram, Thanjavur 613402, India
[b] Department of Chemical Engineering, Indian Institute of Technology Delhi, Hauz kaus, New Delhi 110016, India

Received 1 January 2007; received in revised form 10 August 2007
Available online 31 December 2007

Abstract

Interactions between solids and gas during pneumatic conveying can be utilized for variety of applications including flash drying, solids preheating etc. Experiments on air–solid heat transfer were carried out in a vertical pneumatic conveying heat exchanger of 54 mm inside diameter, using gypsum as the solid material. The effect of solids feed rate (0.6–9.9 g/s), air velocity (4.21–6.47 m/s) and particle size (231–722.5 μm) on air–solid heat transfer rate, heat transfer area and air–solid heat transfer coefficient has been studied. Empirical correlations have been proposed for the prediction of Nusselt number based on the present experimental data. The proposed correlations predict Nusselt number within an error of ±15% for the present data.

Keywords: Air–solid heat transfer; Pneumatic conveying; Dense-phase; Dilute-phase; Nusselt number

1. Introduction

Process industries handle large quantities of materials in powder and granular form during transportation, storage, processing etc. Pneumatic conveying refers to the co-current transportation of solid particles using air/gas at velocities greater than the terminal velocity of particles. Pneumatic conveying finds wide applications in conveying of solids because of the advantages of dust-free transportation, flexibility in routing, ease of maintenance etc. [1]. Gas–solid interactions during pneumatic conveying are widely used to achieve heat transfer between conveying gas medium and solids. Batteries of cyclones with pneumatic conveying ducts between them are widely used to preheat kiln feed in modern cement industries [2]. Drying of free-flowing, heat-sensitive food and pharmaceutical products like animal feed, corn fibers, proteins, antibiotics, enzymes, vitamins, lactose etc. are conveniently done using pneumatic conveying dryers, limiting the exposure time of solids. Hydrodynamics of pneumatic conveying has been widely published [3], whereas studies on gas–solid heat transfer during pneumatic conveying are relatively few. Gas–solid heat transfer experiments in vertical pneumatic conveying duct, using ceramic particles in the size range of 0.7–2.56 mm have been reported and an empirical correlation for gas–solid heat transfer coefficient was also proposed [4]. Data on gas–solid heat and mass transfer for pneumatic drying of alumina, PVC and limestone in industrial dryers have been reported [5,6]. Effect of hydrodynamic parameters on the drying of iron ore in a vertical pneumatic conveying tube has also been reported [7]. Gas-particle heat transfer in spouted beds has been studied where the hydrodynamics in the core are similar to that of dilute-phase pneumatic conveying [8,9]. Gas–solid heat transfer studies in vertical pneumatic conveying at relatively low gas velocities through short, small diameter ducts are scarce in the literature. In the present work, the effects of solids feed rate, particle size and air flow rate on air–solid heat transfer in vertical pneumatic conveying duct at relatively low air velocities are studied and correlations are proposed for the prediction of Nusselt number for gas–solid heat transfer.

* Corresponding author. Tel.: +91 4362 264101; fax: +91 4362 246120.
E-mail address: rajan_sekar@yahoo.com (K.S. Rajan).

0017-9310/$ - see front matter © 2007 Elsevier Ltd. All rights reserved.
doi:10.1016/j.ijheatmasstransfer.2007.09.042

Nomenclature

A_h	heat transfer area (m^2)
a	constant in Eq. (10)
b, c, d	exponents in Eq. (10)
c_p	specific heat of gas (J/kg K)
c_{ps}	specific heat of solid (J/kg K)
d_p	particle diameter (m)
dP	pressure drop across the duct per unit height (N/m^2)
Fe	Federov number (–)
F_m	solid-to-gas mass flow ratio (–)
g	acceleration due to gravity (9.81 m/s^2)
h_p	gas-particle heat transfer coefficient (W/m^2 K)
m_g	mass flow rate of air (kg/s)
m_s	solids feed rate (kg/s)
M_h	solids holdup (kg)
Nu_p	gas-particle Nusselt number (–)
q	rate of air–solid heat transfer (W)
Re_p	particle Reynolds number (–)
$T_{g,in}$	temperature of air leaving the heater (°C)
T_{g1}	steady-state temperature of air at the top of the duct (2.2 m from the bottom) in single-phase flow (°C)
T_{g2}	steady-state temperature of air at the top of the duct (2.2 m from the bottom) in air–solid flow (°C)
T_{s2}	solids exit temperature at the top of the duct (°C)
T_{s1}	inlet solids temperature (°C)
v_a	average velocity of air (m/s)

Greek symbols

μ_a	viscosity of air (kg/ms)
ρ_a	density of air (kg/m^3)
ρ_s	density of solid (kg/m^3)
ΔT	log-mean temperature difference (K)

2. Experimental setup

A schematic diagram of the experimental setup is shown in Fig. 1. The experimental setup consists of a blower (max discharge – 600 L/min at normal temperature and pressure, manufactured by Ramdeep Industries), a heating section comprising a 100 mm inner diameter G.I. air duct fitted with three electrical heaters of 5 kW total heating capacity, a horizontal section consisting of an orifice meter and solids feeding system, a pneumatic conveying duct and a cyclone separator for the collection of solids. Flow rate of air entering the heating section is controlled using bypass valves BV1 and BV2 located at the discharge of blower. The heaters are capable of heating air to a temperature of 180 °C at the maximum rated blower capacity. A horizontal section made of 54 mm inner diameter galvanized iron pipe is connected to the heating section. An orifice meter connected to a U-tube manometer, has been fitted in this horizontal section and is used to measure the air velocity and its flow rate. Inlet air temperature is measured on the downstream side of the orifice meter and is maintained using a digital relay temperature controller. The solids feeding system consists of a venturi and a double-cone arrangement. Venturi has been designed in such a way that the solids entering the throat of venturi are rapidly carried by gas at the expense of smaller pressure loss. Upstream cone (converging section) of the venturi is 50 mm long. Inner diameter of the throat is 25 mm. A circular hole of 15 mm diameter has been made at the centre of the throat. To avoid boundary layer separation and ensure recovery of pressure in the diverging section, the angle of diverging cone should be less. Hence the downstream cone (diverging section) has been made longer than the upstream cone and is 100 mm long. This venturi ejector has been fitted inside the horizontal pipe and welded to hold the same in position. A hole has been made on the horizontal pipe encapsulating the venturi in such a way that this hole is inline with the hole drilled in the throat of venturi. A short, mild steel pipe of 12 mm inner diameter connects the hole in the throat of venturi and the hole on the horizontal pipe. The other end of mild steel pipe protrudes outside the portion of the duct encapsulating the venturi.

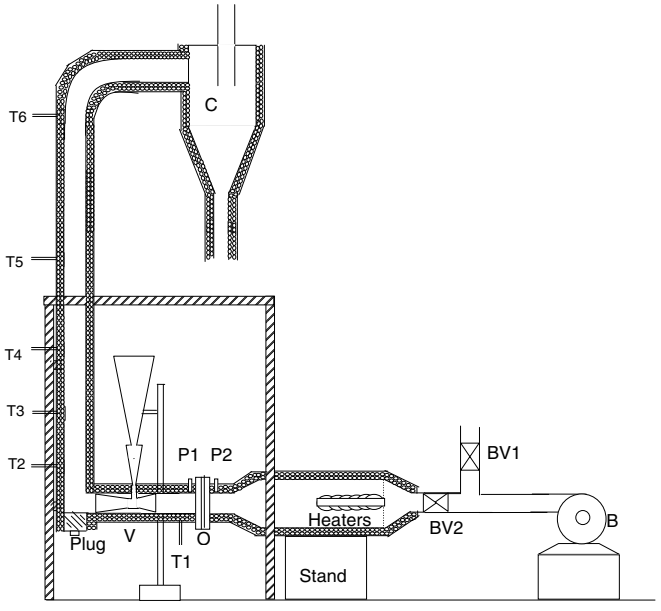

T1: Thermocouple for digital relay controller; T2-T5: 'K' type thermocouples connected to six-way indicator; T6: 3-wire RTD; C: Cyclone separator; V: Venturi for solid feeding; BV1, BV2: Bypass valves; B: Blower; O: Orifice plate; P1, P2: Pressure taps

Fig. 1. Schematic diagram of the experimental setup.

Five smooth-walled aluminum cones with different orifice sizes between 3 mm and 10 mm at the bottom have been used to deliver solids to the venturi. One of such cones has been attached to the open end of the mild steel pipe leading to the throat of venturi. A bigger cone (also made of smooth aluminum sheet) with a larger opening at the apex is supported by a stand and is placed over the smaller cone, in such a way that a portion of the larger cone is immersed in the smaller cone. At the onset of solids feeding, solids fed to the larger cone enter the smaller cone at a rate faster than the rate at which solids are delivered from the smaller cone to the throat. This leads to lower cone getting rapidly filled with solids till the solids level reaches the apex of upper cone. Once this condition is attained, rate of discharge of solids from upper cone to lower cone and that from lower cone to the throat of venturi are same maintaining a constant level of solids in the smaller cone thereby circumventing the role of solids head on the feed rate of solids.

Horizontal section consisting of venturi, heater and blower is connected to the vertical duct with a 'Tee' whose lower end in the vertical section is closed by a plug. This facilitates withdrawal of solids collected in the duct and measurement of its mass to determine solids holdup in the vertical duct. When tightened, the top surface of the plug coincides with the level of the horizontal section preventing the formation of dead zones at the bottom of the duct. The distance between the venturi and the vertical duct is kept at a minimum value to minimize heat transfer before entry to vertical duct. The vertical duct is 54 mm inner diameter G.I. pipe of 2.3 m high, fitted with five thermocouples at various axial locations to measure axial air temperature profile.

The sensing part of thermocouples is covered with a brass mesh to prevent the access of solids to hot junction and hence the thermocouples indicate air temperature. Three-wire RTD located at the top of the duct at the axial location of 2.2 m is used to measure air exit temperature. During flow, solids are collected in the bin located at the bottom of cyclone at solids exit. The whole experimental setup is insulated using two layers of asbestos rope wound around them and covered with a paste of magnesia–asbestos mixture to prevent heat loss. Additional insulation is provided to the vertical duct using a layer of glass wool covered by a thin aluminum sheet.

3. Experimental procedure

A typical experimental procedure consists of adjusting air flow rate using the bypass valves to achieve the desired air flow rate and then switching the heaters on. Axial temperature profiles in the duct are monitored periodically to check for the attainment of steady state. Once the steady state with air flow is attained, temperature of air leaving the heater ($T_{g,in}$) and air temperature at the top of the vertical duct (T_{g1}) are noted. Solids feed of a particular size, carefully screened is fed manually to the top cone. Solids leaving the top cone reach the lower cone and subsequently enter the small duct leading to the throat of venturi. The larger orifice of the top cone ensures that the lower cone is rapidly filled and solids height in the lower cone is maintained. To ensure that the double-cone arrangement delivers solids at a constant rate, a series of 'mass of solids discharged' versus 'time' data were collected for a few representative particle sizes and orifice sizes of the lower cone, by discharging particles from double-cone arrangement to ambient air. The observations indicated that the double-cone arrangement is capable of delivering solids at a constant rate, though the data are not shown here for brevity.

Axial temperature profiles are monitored periodically during air–solid flow to ascertain the steady state. Any fluctuation in the solids feed rate is likely to affect the axial air temperature profiles and the air exit temperature. Hence monitoring the axial temperature profile ensures steady feeding of solids to the horizontal duct and also helps to ascertain steady state. Once the steady state with air–solid flow is reached, temperature of air at the top of the vertical duct (T_{g2}) is noted. Solids feed rate depends on the orifice size of the lower cone, particle size and air flow rate and hence a unique solids feed rate is obtained for a combination of these three factors. Solids feed rate is determined by noting the time taken for conveying predetermined mass of solids.

Solids holdup or solid volume concentration needs to be determined to estimate heat transfer area in pneumatic conveying heat exchanger. A few investigators have used quick-closing valves to determine the mass of solids trapped in the duct and hence the solids holdup. In this study, solids holdup is determined through simultaneous shutting of air flow and solids feed (achieved by switching the blower off at the instant of disappearance of solids from the lower cone). Solids present in the vertical duct at that instant would be collected at the bottom of the duct, which can be collected by opening the plug at the bottom of Tee. Mass of the collected solids gives solids holdup, a measure of average solid concentration in the duct. Similar procedure has been followed for determination of solids holdup in cyclone heat exchanger [2,10]. Since the method of determination of solids holdup is prone to errors, holdup measurements were repeated three times to ensure reproducibility.

Large quantities of gypsum were sieved over a set of British Standard Sieves (BSS) and material retained on each sieve was collected. Particle size of solids retained on each sieve is the arithmetic average of mesh size corresponding to the sieve on which the solids are retained and the mesh size of the sieve immediately above it. Each particle size fraction has been collected and carefully stored in closed plastic containers capable of holding 5 kg of solids. Care has been taken to avoid entry of foreign materials such as dust and non-spherical particles as they would interfere during the solids flow and would even choke the solids flow. Table 1 shows the calculation of particle sizes investigated here. Table 2 shows the range of variables

Table 1
Particle sizes investigated in the present study

S. no	BSS screen no.		Sieve opening (μm)		Average particle size (μm)
	Overflow	Underflow	Overflow	Underflow	
1	18	25	845	600	722.5
2	25	30	600	495	547.5
3	30	36	495	425	460.0
4	36	44	425	355	390.0
5	60	72	250	212	231.0

Table 2
Range of variables investigated

S. no	Variable	Value
1	Particle size	231, 390, 460,547.5 and 722.5 μm
2	Air velocity	4.21–6.47 m/s
3	Solid feed rate	0.6–9.9 g/s

Table 3
Physical properties of the solid investigated

S. no	Property	Value
1	Density	2317 kg/m^3
2	Specific heat	1090 J/kg K
3	Thermal conductivity	0.17 W/m K

and Table 3 shows the relevant properties of the solid investigated. Table 4 presents the variables measured, instruments used and uncertainty involved in their measurements.

4. Results and discussion

Heat transfer from gas to solid involves two steps: Transfer of heat from bulk of the gas to the surface of the solid across the gas film surrounding the solid (External resistance) and the propagation of heat through conduction within the particle to reach isothermal condition within the particle (Internal resistance). Internal resistance controls the heat transfer if Biot number (ratio of internal to external resistance) is greater than 20. For the particle sizes under study, the high thermal conductivity of solids results in Biot number less than 0.25, leading to gas-film resistance controlled problem [11]. Hence the resistance to heat transfer can be assumed to rest solely with the gas film surrounding the particle. The gas–solid heat transfer coefficient is defined as

$$h_p = \frac{q}{A_h \Delta T} \tag{1}$$

Measurement of solids temperature has been a challenge, especially in the duct where particles are inseparable from air during measurement of temperature. While a thermometer placed in the storage bin indicates solids inlet temperature, the exit temperature of solids is determined by means of a thermal balance from the heat transferred from the gas to solids. For this purpose and to exclude the heat loss due to poor insulation at the bottom of the Tee, gas–solid heat transfer rate is calculated from the difference in steady-state temperature of the air at the top of the duct (at the axial location of 2.2 m), before and after feeding the solids. Hence,

$$q = m_g c_p (T_{g1} - T_{g2}) \tag{2}$$

where T_{g1} and T_{g2} are steady-state temperatures of air at the top of the duct in the single-phase flow and air–solid flow, respectively. This difference is temperature of air is attributed to the heat transfer from hot air to cold solids feed and hence is a measure of gas–solid heat transfer. Specific heat of gas is estimated at the average of temperatures, T_{g1} and T_{g2}. The effect of presence of particles on gas-wall heat transfer may be neglected for the particle sizes and solid-loading ratios (solid-to-air flow rate ratio) investigated in the present study. Hence, the exit solids temperature is calculated as follows:

$$T_{s2} = T_{s1} + \frac{q}{m_s c_{ps}} \tag{3}$$

Since the gas and solids move parallel in same direction, the vertical pneumatic conveying duct can be considered as 1-1, co-current heat exchanger. Accordingly ΔT in Eq. (1) is the log-mean temperature difference defined as

$$\Delta T = \frac{(T_{g,in} - T_{s1}) - (T_{g2} - T_{s2})}{\ln\left(\frac{T_{g,in} - T_{s1}}{T_{g2} - T_{s2}}\right)} \tag{4}$$

Assuming particles to be spherical, heat transfer area (A_h) is the surface area of the particles in the duct at any instant

Table 4
Measured quantities, instruments used, least counts and uncertainties involved

Quantity measured	Instrument used	Least count	Uncertainty involved
Air temperature at the downstream of orifice	K-type thermocouple with digital indicator	±1 °C	±1 °C
Air temperature at various axial locations in the duct	K-type thermocouple with six-way 31/2 digital indicator	±1 °C	±1 °C
Air temperature at the top of the duct (at 2.2 m from the bottom of the duct)	3-Wire RTD with 41/2 digital indicator	±0.1 °C	±0.1 °C
Feed solid temperature	Mercury in glass thermometer	±0.5 °C	±0.5 °C
Pressure drop across orifice	U-tube manometer	±1 mm	±1 mm
Mass of solid for feed rate measurement	Digital Balance	±0.1 g	±1 g
Mass of solid for holdup measurement	Digital Balance	±0.001 g	±0.1 g
Time	Digital stop watch	±1 s	±1 s

of time related to the holdup (M_h), density (ρ_p) and size of the particles (D_p) as

$$A_h = \frac{6M_h}{\rho_s D_p} \tag{5}$$

Solids holdup is an essential parameter in the analysis of pneumatic conveying duct as heat exchanger. Experimental determination of heat transfer coefficient, a widely used design parameter for heat exchangers requires the knowledge of heat transfer area. In conventional heat exchangers, the heat transfer area is fixed from the dimensions and the geometry of heat exchanger. In pneumatic conveying heat exchangers, the heat transfer area depends on the average solid concentration or solids holdup in the duct.

4.1. Effect of solids feed rate on air–solid heat transfer rate and air–solid heat transfer coefficient

Experiments were conducted with uniform size particles at a constant air velocity for different solids feed rates to study the effect of solids feed rate on various aspects of air–solid heat transfer. Since solids holdup in the duct plays an important role in determining the heat transfer area, the effect of solids feed rate on solids holdup has also been studied. Fig. 2 shows the effect of solids feed rate on solids holdup for 547.5 μm size particles at the air velocity of 5.8 m/s. It can be observed from Fig. 2 that the solids holdup increases with solids feed rate till a certain solids feed rate, after which solids holdup begins to remain constant. This can be explained as follows: For a fixed particle size and air velocity, an increase in solids feed rate results in increase in number of particles in the duct leading to higher solid volume concentration and hence higher mass of solids in the duct. Hence solids holdup increases with solids feed rate.

At a constant solids flux, with decreasing gas velocity or at a constant gas velocity with increasing solids flux, different flow regimes exist in upward gas–solid flow in a duct. A flowchart and a flow regime diagram depicting the transition between different regimes in vertical pneumatic conveying is available [12]. At a constant gas velocity at low solids feed rates, the duct may operate under dilute-phase flow regime wherein the solid concentration practically remains constant along the duct height, but changes with solids feed rate. With gradual increase in solids feed rate, a transition in the flow regime from dilute-phase to fast fluidization would take place leading to two zones in the duct: A dense-phase zone at the bottom where solid concentrations are high and a dilute-phase zone at the top with low solid concentrations. The phenomenon representing the onset of occurrence of a dense bed at the bottom of the pneumatic conveying duct is called accumulative choking or Type A choking [12]. This occurs when the gas velocity is insufficient to maintain all the particles fully in suspension in the entire duct. This phenomenon is different from Type C or classical choking which is attributed to occurrence of slug flow and flow instability [12].

With further increase in solids feed rate, height of the dense bed continues to increase [13–15] or axial location demarcating dense and dilute bed regions moves up. Different axial locations of the duct will attain fully dense condition at different solids feed rates for a fixed particle size and gas velocity [16]. This solids feed rate representing the transition to fully dense bed depends on particle and gas properties, particle size, gas flow rate, duct geometry etc. [17]. The variation of solids holdup with solids feed rate is expected to be small once dense bed is formed [16]. The transition solids feed rate can be determined from the plot of apparent solids holdup versus solids feed rate. Transition solids circulation rate in a circulating fluidized bed was determined as the solids circulation rate at which solids holdup levels off [16]. This was indicated as the starting point of fully dense conditions in the bed. Hence in the range of solids feed rates investigated in the present study where constant solids holdup has been observed, the duct is expected to be operating in the dense-phase regime, while

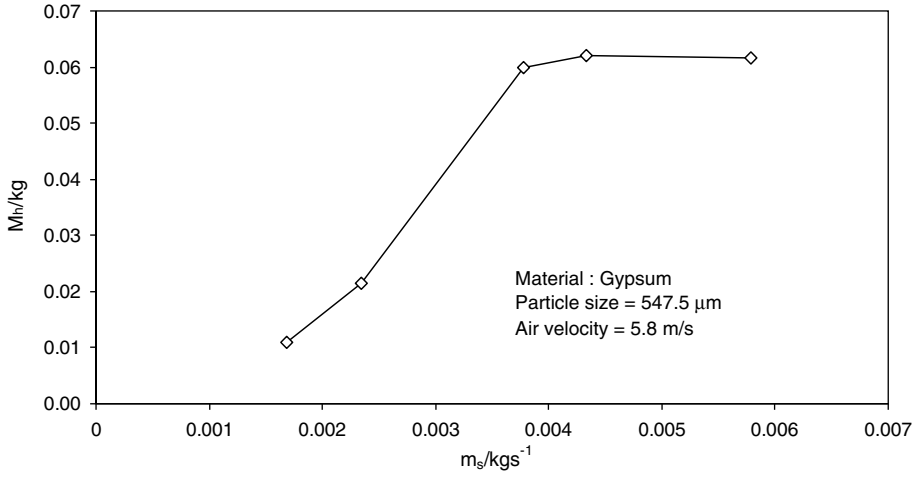

Fig. 2. Variation of solids holdup with solids feed rate.

dilute-phase or fast-fluidization regime exists in the range of solids feed rates where solids holdup increases with solids feed rate. This probably explains the observation in the present study with respect to effect of solids feed rate on solids holdup especially at higher solids feed rates. Small fluctuations in solids holdup in dense-phase regime may be attributed to changes in air velocity due to heat transfer. At higher gas velocities, formation of dense bed is shifted to higher solids feed rates and vice versa.

The presence of dense bed throughout the duct height may also be confirmed by studying the effect of solids feed rate on pressure drop in the duct at these solids feed rates. A plot showing the effect of solids feed rate on axial pressure drop in the duct (with pressure taps at the axial location of 0.3 and 2.2 m) is shown in Fig. 3 for the same solid and air inlet temperatures. It may be observed from Fig. 3 that the pressure drop increases initially with solids feed rate and then begins to remain constant. This has confirmed the existence of dense bed in the entire duct at higher solids feed rates. Though pressure drop measurements were made, solid volume concentrations have not been estimated using pressure drop since the acceleration region may not have been included. Also, it has been highlighted that the pressure drop method for estimation of solids volume concentration is prone to errors at low solids feed rates in small diameter ducts [3].

Fig. 4 shows the effect of solids feed rate on air–solid heat transfer rate while conveying cold particles of size 547.5 μm at the air velocity of 5.8 m/s. It is evident from Fig. 4 that air–solid heat transfer rate increases with solids feed rate. This observation can be explained as follows: Air–solid heat transfer rate depends on heat transfer area, which is a function of solids holdup. Since solids holdup increases with increase in solids feed rate as evident from Fig. 2, heat transfer area and air–solid heat transfer rate increase. Also with increase in solids feed rate, increase in solids temperature is expected to be less due to higher heat capacity (product of solids feed rate and specific heat capacity), leading to increased driving force locally. Hence a combination of high heat transfer area and increase in driving force results in higher air–solid heat transfer rate with increase in solids feed rate. This supports the observa-

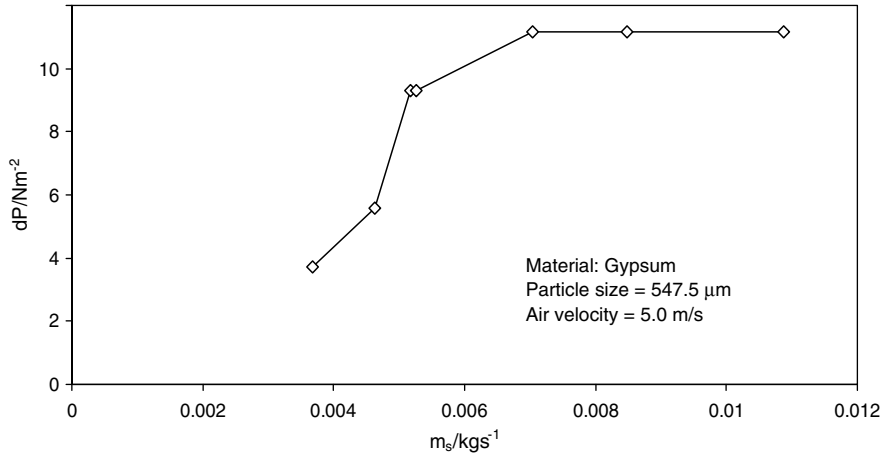

Fig. 3. Variation of duct pressure drop per unit height with solids feed rate.

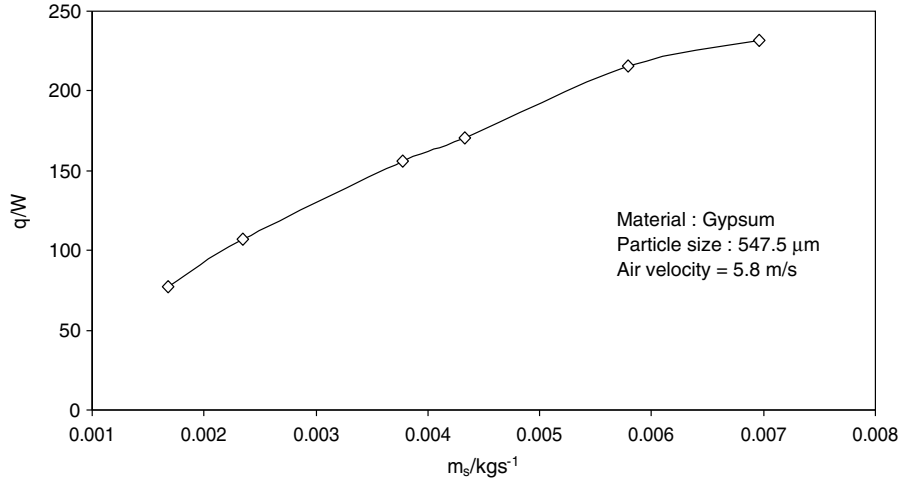

Fig. 4. Effect of solids feed rate on air–solid heat transfer rate for 547.5 μm size particles.

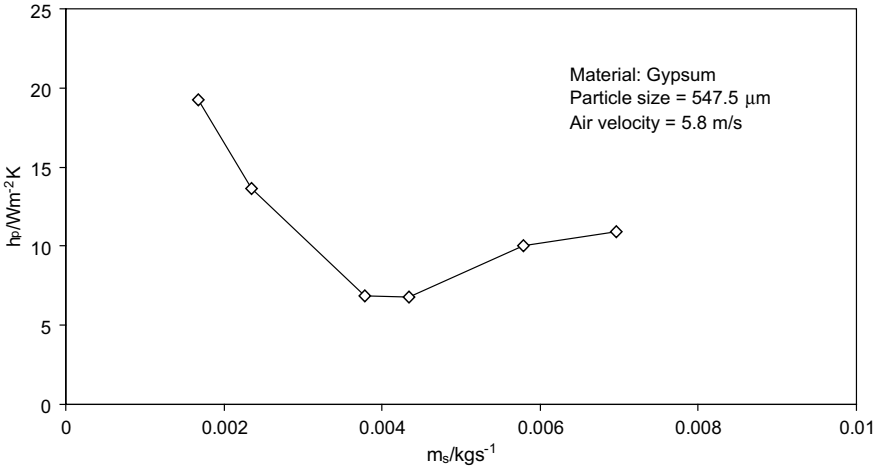

Fig. 5. Effect of solids feed rate on air–solid heat transfer coefficient for 547.5 μm size particles.

tion in Fig. 4, where air–solid heat transfer rate increases continuously with solids feed rate, despite nearly constant heat transfer area at higher solids feed rates. Increase in gas–solid heat transfer rate in the spout region of spouted bed with increase in solids feed rate has been reported [8] and the same has been attributed to increase in solids volume concentration in the spout with increasing solids feed rate. This supports the observations in the present study on the effect of solids feed rate on air–solid heat transfer rate.

Fig. 5 shows the variation of air–solid heat transfer coefficient with solids feed rate at the air velocity of 5.8 m/s for 547.5 μm particles. It can be observed from Fig. 5, that the air–solid heat transfer coefficient decreases with solids feed rate at low solids feed rates, while it increases with solids feed rate at higher solids feed rates. This can be explained as follows:

From Eq. (1), it is evident that air–solid heat transfer coefficient is directly proportional to air–solid heat transfer rate and inversely proportional to the product of heat transfer area and log-mean temperature difference. As explained in previous paragraphs, air–solid heat transfer rate increases with solids feed rate for the entire range of solids feed rates. However, in the range of solids feed rates corresponding to the existence of dilute-phase and fast-fluidization regimes, solids holdup and hence the heat transfer area increases with solids feed rate. The increase in heat transfer area with solids feed rate is higher than the increase in air–solid heat transfer rate with solids feed rate. This larger increase in heat transfer area nullifies the increase in air–solid heat transfer rate with solids feed rate. Hence in the range of solids feed rates corresponding to dilute-phase and fast-fluidization regimes, air–solid heat transfer coefficient decreases with solids feed rate due to reduction in the ratio of air–solid heat transfer rate to heat transfer area with increase in solids feed rate.

When the duct is operated in the dense-phase regime, heat transfer area remains nearly constant with solids feed rate, while air–solid heat transfer rate still increases with the solids feed rate. This is due to the fact that the solids holdup does not change appreciably with solids feed rate in the dense-phase regime. The maximum solid loading ratio (ratio of solid to gas mass flow rates) in the present study is 0.9 and hence all particle–particle collisions and fragmentation can be ignored. Hence the air–solid heat transfer coefficient increases with solids feed rate in the dense-phase regime due to increase in air–solid heat transfer rate and nearly constant heat transfer area.

Decrease in gas-particle heat transfer coefficient with increasing solid volume concentration in the range between 0.00025 and 0.05 has been observed for heat transfer between air and ceramic particles [4]. This observation from experiments carried out at higher gas velocities than that used in the present study support the findings of the present study in the dilute/fast-fluidization regime where solids holdup and solid volume concentration increase with solids feed rate and accordingly heat transfer coefficient decreases with solids feed rate and solids holdup.

4.2. Effect of particle size on air–solid heat transfer rate and air–solid heat transfer coefficient

With the solids feeding system used in the present study, solids feed rate depends on the orifice size of the lower cone, particle size and air velocity. Solids feed rate could not be maintained at the same value for different particle sizes at a constant air velocity, even with the use of lower cones of different orifice sizes. Hence the effect of particle size on air–solid heat transfer is studied as a function of solids feed rate at a constant air velocity. Fig. 6 shows the variation of solids holdup with particle size as a function of solids feed rate at the air velocity of 5.8 m/s. It is clear from Fig. 6 that solids holdup increases with particle size for a solids feed rate at a constant air velocity. This observation can be explained as follows: Acceleration of particles in pneumatic conveying is mainly due to the drag force between air and solids. Larger particles have lower drag in pneumatic conveying [18] and hence lower acceler-

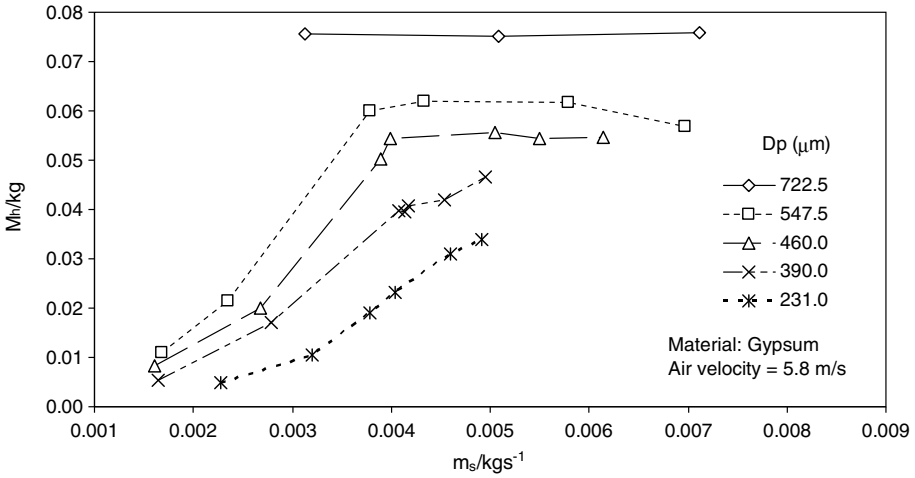

Fig. 6. Effect of particle size on solids holdup at different solids feed rates for the air velocity of 5.8 m/s.

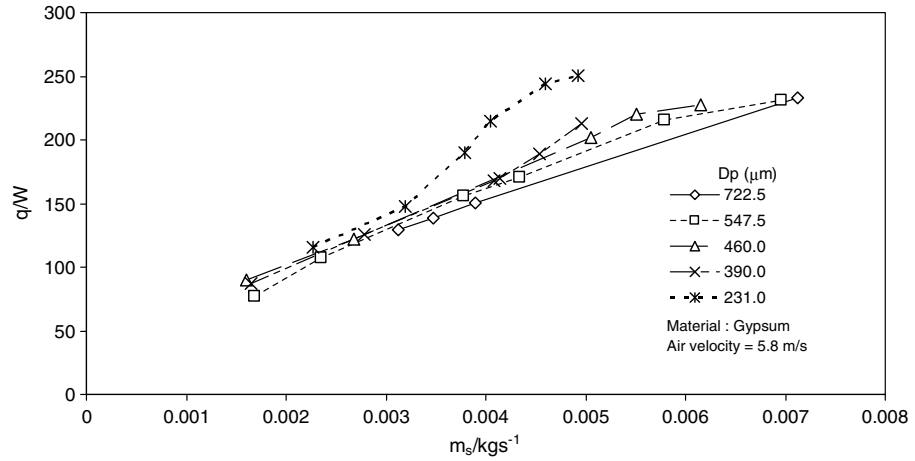

Fig. 7. Variation of air–solid heat transfer rate with particle size at different solids feed rates for the air velocity of 5.8 m/s.

ation resulting in higher holdup of solids. Hence solids holdup increases with increase in particle size.

Fig. 7 shows the effect of particle size on air–solid heat transfer rate at different solids feed rates for the air velocity of 5.8 m/s. It can be observed from Fig. 7 that air–solid heat transfer rate is not a strong function of particle size initially, while tangible effect of particle size on air–solid heat transfer rate can be observed at higher solids feed rates, where heat transfer rate decreases with particle size. The effect of particle size on air–solid heat transfer rate depends on effect of particle size on heat transfer area and the driving force for heat transfer. With increase in particle size, solids holdup increases while the particle surface area per unit volume decreases which influence the heat transfer area. Accordingly a plot of heat transfer area for different size particles as a function of solids feed rate at the air velocity of 5.8 m/s is made in Fig. 8. Fig. 8 shows that heat transfer area as calculated from Eq. (5) increases with particle size at lower solids feed rates, while at higher feed rates (corresponding to dense-phase regime) heat transfer area decreases with particle size. At constant air velocity and solids feed rate, increase in heat transfer area would result in higher heat transfer rates in the initial portions of the duct, while decreasing the driving force for heat transfer in the later portions of the duct. The reverse holds true if the heat transfer area is less. Since heat transfer rate is calculated over the entire height of duct, varying heat transfer rates at various positions along the duct for different particle sizes would have resulted in nearly same average air–solid heat transfer rate for the entire height of the duct at lower solids feed rates. At higher solids feed rates, the combination of heat transfer area and driving force in the duct may be such that the average air–solid heat transfer rate decreases with particle size.

Fig. 9 shows the effect of particle size on air–solid heat transfer coefficient as a function of solids feed rate at the air velocity of 5.8 m/s. It can be observed from Fig. 9 that the air–solid heat transfer coefficient decreases with particle size in dilute-phase conveying regime. This can be attributed to the fact that air–solid heat transfer rate is nearly independent of particle size, while the heat transfer area increases with particle size due to increased solids holdup

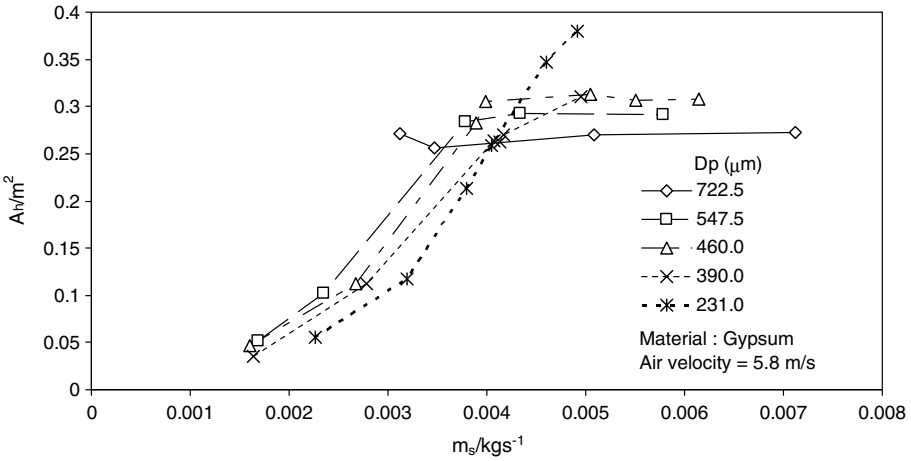

Fig. 8. Variation of heat transfer area with particle size at different solids feed rates for the air velocity of 5.8 m/s.

for large particles as evident from Fig. 8. This results in lower air–solid heat transfer coefficient for large particles. For particles in the dense-phase regime, air–solid heat transfer coefficient is nearly independent of particle size since both the air–solid heat transfer rate and heat transfer area decrease with particle size. Hence it may be concluded that the air–solid heat transfer coefficient decreases with particle size at low solids feed rates typical of dilute or fast-fluidization regimes, while the effect of particle size on air–solid heat transfer coefficient is negligible at higher solids feed rates.

4.3. Effect of air velocity on air–solid heat transfer rate and air–solid heat transfer coefficient

The effect of air velocity on air–solid heat transfer rate has been studied by using solids of a single size at nearly same solids feed rate at different air velocities. Fig. 10 shows the variation of air–solid heat transfer rate with air velocity plotted in terms of solids feed rate for particles of 547.5 μm. It can be seen from Fig. 10 that the air–solid heat transfer rate increases with air velocity in the range between 4.3 m/s and 5.8 m/s, after which the air–solid heat transfer rate decreases with air velocity as seen for the air velocity of 6.3 m/s. This is observed for other particle sizes also (though results are not shown here). To understand this phenomenon, plots of variation of solids holdup with air velocity at different solids feed rates are made in Fig. 11 for 547.5 μm size particles. For particles of constant size at higher air velocity, relative velocity between air and solid phases is high, leading to larger drag. Increased drag leads to increase in solids velocity or a decrease in solid concentration leading to reduced solids holdup at higher air velocities. Reduced solids holdup for a fixed particle size indicates reduced heat transfer area. But, increase in air velocity results in the presence of more amount of high temperature air. The later results in increase in air–solid heat transfer rate while the former leads to decrease in air–solid heat transfer rate. The relative influence of the two factors determines the effect of air velocity on air–solid heat transfer rate. Hence with increase in air velocity, air–solid heat transfer rate increases initially when large heat capacity of air offsets decrease in heat transfer area. At an air velocity of 6.3 m/s it seems that the decrease in heat

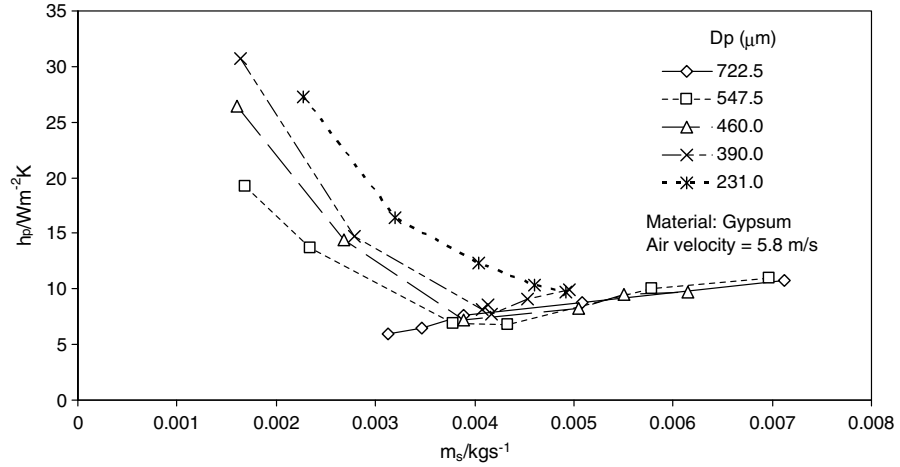

Fig. 9. Effect of particle size on air–solid heat transfer coefficient at different solids feed rates for the air velocity of 5.8 m/s.

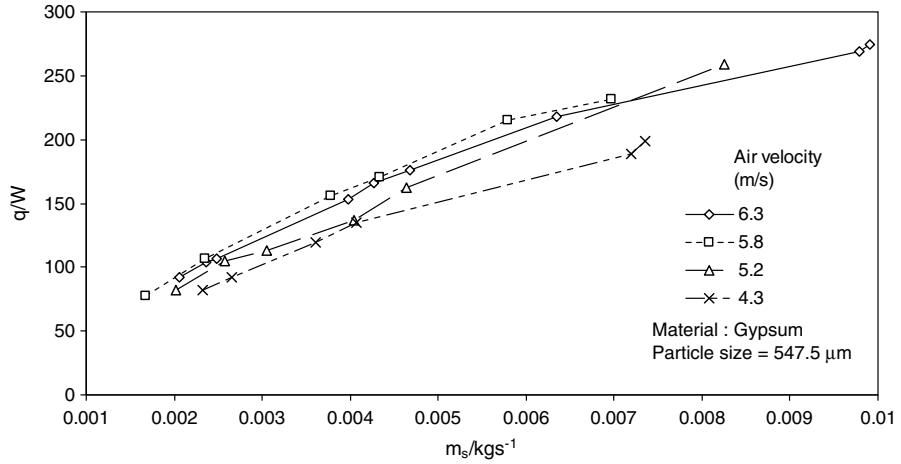

Fig. 10. Effect of air velocity on air–solid heat transfer rate for 547.5 μm particles at different solids feed rates.

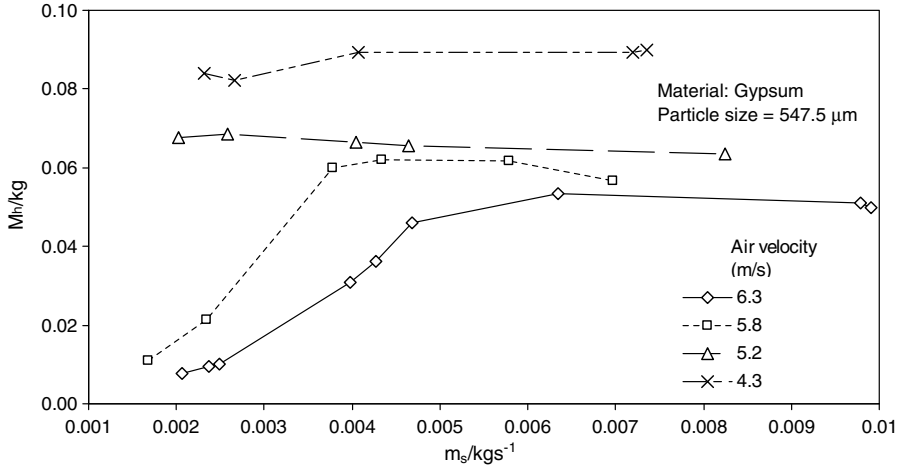

Fig. 11. Variation of solids holdup with air velocity at different solids feed rates for particles of 547.5 μm diameter.

transfer area overcomes the effect of higher heat capacity of air and hence air–solid heat transfer rate is lower than that compared at the air velocity of 5.8 m/s.

Fig. 12 shows the variation of air–solid heat transfer coefficient with air velocity at different solids feed rates for 547.5 μm size particles. It can be observed from

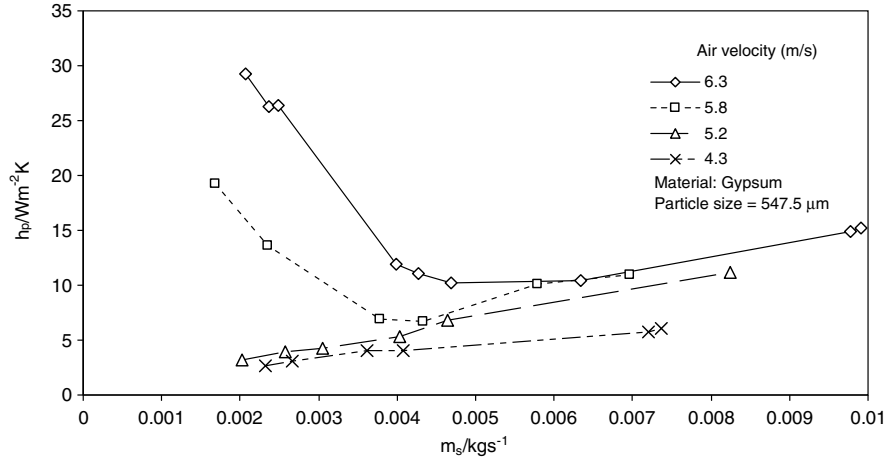

Fig. 12. Effect of air velocity on air–solid heat transfer coefficient at different solids feed rates for particles of 547.5 μm diameter.

Fig. 12 that air–solid heat transfer coefficient increases with increase in air velocity. As discussed earlier, air–solid heat transfer rate increases with air velocity till the air velocity of 5.8 m/s while the heat transfer area decreases continuously. Increase in air–solid heat transfer rate coupled with reduction in heat transfer area results in increase of air–solid heat transfer coefficient with air velocity in this range. At an air velocity of 6.3 m/s though the air–solid heat transfer rates are lower than that at 5.8 m/s, heat transfer coefficients are higher due to large reduction in solids holdup and hence the heat transfer area. This phenomenon is observed for other particles sizes as well. Hence it may be concluded that the air–solid heat transfer coefficient increases with increase in air velocity for the range of air velocities investigated here.

Increase in gas-particle heat transfer coefficient with gas velocity has been observed in the literature as well [4]. An optimum air velocity corresponding to a maximum in gas-particle heat transfer coefficient has been observed for pneumatic drying of alumina [19]. Though no explanation for this behaviour was provided, this could be attributed to the following:

At higher gas velocities reported in [19], very low concentration of solids may have led to extremely lower heat transfer rate and hence gas-particle heat transfer coefficient would have been found to decrease with increase in gas velocity despite lower heat transfer area.

5. Development of correlation for gas-particle heat transfer coefficient

Nusselt number, particle Reynolds number and Prandtl number have been widely used to correlate gas-particle heat transfer coefficient. Prandtl number does not vary significantly over the range of air temperatures used in the present study and hence it has not been included in the development of correlation. Terminal velocity has been used as the characteristic velocity in particle Reynolds number of a few correlations for gas–solid heat transfer reported in the literature for pneumatic drying, while gas velocity has been used as characteristic velocity in other correlations [4,5]. Superficial air velocity is a variable that can be determined easily and it plays an important role in determining the hydrodynamics and heat transfer as discussed in previous sections. Hence superficial air velocity is taken as characteristic velocity in the definition of Reynolds number for the present study. Accordingly, the dimensionless numbers are defined as follows:

$$Nu_{\mathrm{p}} = \frac{h_{\mathrm{p}} d_{\mathrm{p}}}{k_{\mathrm{a}}} \tag{6}$$

$$Re_{\mathrm{p}} = \frac{d_{\mathrm{p}} v_{\mathrm{a}} \rho_{\mathrm{a}}}{\mu_{\mathrm{a}}} \tag{7}$$

Since the solids feed rate affects air–solid heat transfer coefficient considerably, it is incorporated as dimensionless ratio of solids to air mass flow rate (F_{m}) as

$$F_m = m_{\mathrm{s}}/m_{\mathrm{a}} \tag{8}$$

In addition, Nusselt number is considered as a function of Fedorov number as proposed by Ludera [20]. Fedorov number is a function of particle size and physical properties of air and solid particles as given below:

$$Fe = d_{\mathrm{p}} \left[\frac{4 g \rho_{\mathrm{a}}^2}{3 \mu_{\mathrm{a}}^2} \left(\frac{\rho_{\mathrm{s}}}{\rho_{\mathrm{a}}} - 1 \right) \right]^{1/3} \tag{9}$$

A rapid decrease in air–solid heat transfer coefficient with solids feed rate is observed at low solids feed rates while at solids feed rates beyond a certain value, air–solid heat transfer coefficient increases with increase in solids feed rate. Similarly, at lower solids feed rates air–solid heat transfer coefficient decreases with increase in particle size while the same is nearly independent of particle size at higher solids feed rates. To accommodate these significant behavioral changes at a transition solids feed rate for a fixed particle size and average air velocity, two different correlations of the following form have developed.

$$Nu_{\mathrm{p}} = a Re_{\mathrm{p}}^{b} F_{\mathrm{m}}^{c} Fe^{d} \tag{10}$$

The values of coefficient and exponents depend on the regime of transport. As discussed earlier, the transition solids feed rate depends on gas and solid properties, gas flow rate, particle size, bed geometry, etc. The literature data to determine the transition solids feed rate shows much scatter [16] indicating the difficulty in proposing a single correlation for its determination applicable for all cases. Hence correlation for predicting transition solids feed rate is not developed in the present study but separate correlations of the form of Eq. (10) for determination of Nusselt number is proposed for dilute/fast-fluidization regime and dense-phase regime, in such a way that the same may be used depending upon the regime of operation.

The coefficient (a) and exponents (b, c and d) for two regimes have been evaluated by regression analysis for the present experimental data having solids to air loading ratio range from 0.09 to 0.87 and Fedorov number range from 8.28 to 26.79, particle Reynolds number range from 36.59 to 175.33 and Nusselt number range from 0.0212 to 2.189. Statistical significance of the correlation coefficients a, b, c and d were determined by Student t-test. Corresponding 'P' values were closer to zero. Regression coefficients are said to be statistically significant, if the 'P' values are lesser than 0.05 at 95% confidence level. The resulting correlations are

For dilute-phase/fast-fluidization regime:

$$Nu_{\mathrm{p}} = 8.2951 \times 10^{-7} Re_{\mathrm{p}}^{5.3365} F_m^{-1.3863} Fe^{-5.0530} \tag{11}$$

For dense-phase regime:

$$Nu_{\mathrm{p}} = 1.3360 \times 10^{-4} Re_{\mathrm{p}}^{2.7624} F_{\mathrm{m}}^{0.6792} Fe^{-1.8344} \tag{12}$$

Nusselt numbers predicted by Eqs. (11) and (12) are compared with experimental values in Figs. 13 and 14. Eqs. (11) and (12) predict Nusselt numbers within an error +15% to

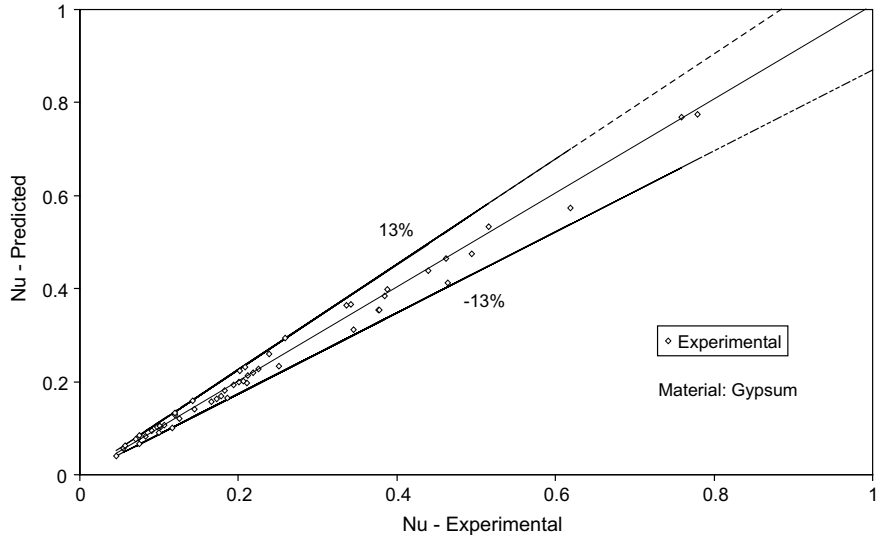

Fig. 13. Comparison of Nusselt numbers predicted from Eq. (11) with experimental values.

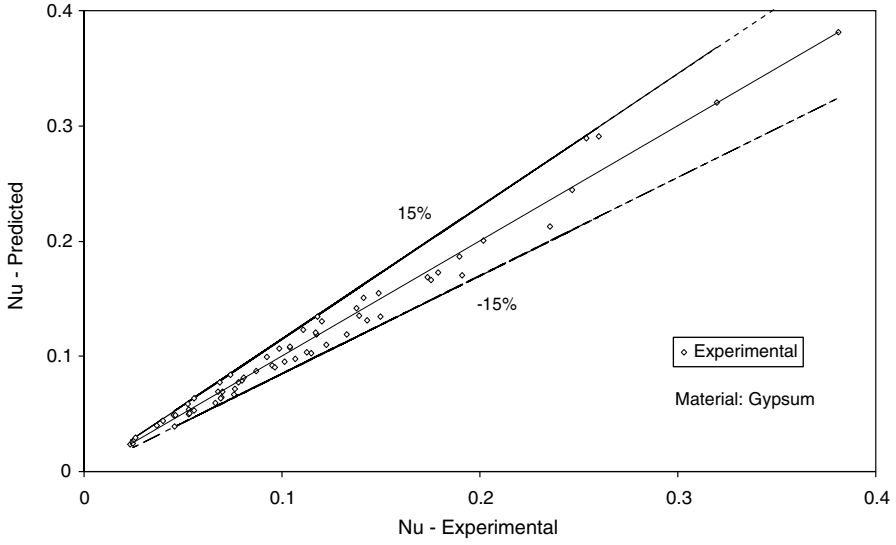

Fig. 14. Comparison between Nusselt numbers predicted from Eq. (12) and experimental values.

−15% with correlation coefficients of 0.99 and 0.98, respectively.

6. Conclusions

Air–solid heat transfer rate increases with increasing solids feed rate, while the same increases initially with air velocity and undergoes a maximum before decreasing with increase in air velocity. Gas-particle heat transfer coefficient decreases with solids feed rate at lower solids feed rates typical of dilute/fast-fluidization regime. Gas-particle heat transfer coefficient increases with solids feed rate at higher solids feed rates and increases with air velocity at all solids feed rates. The proposed correlations predict the particle Nusselt number of the present study within an error of +15% to −15%.

Acknowledgement

The first and third authors acknowledge the Vice Chancellor, SASTRA for his support for this work.

References

[1] O. Molerus, Overview: pneumatic transport of solids, Powder Technol. 88 (1996) 309–321.
[2] A. Jain, B. Mohanty, B. Pitchumani, K.S. Rajan, Study of gas–solid heat transfer in cyclone heat exchanger, ASME J. Heat Transfer 128 (8) (2006) 761–768.
[3] V. Poikoainen, A. Rautiainen, G. Stewart, P. Sarkomaa, An experimental study of vertical pneumatic conveying, Powder Technol. 104 (1999) 139–150.
[4] J. Bandrowski, G. Kaczmarzyk, Gas-to-particle heat transfer in vertical pneumatic conveying of granular materials, Chem. Eng. Sci. 33 (1976) 1303–1310.

[5] J. Baeyens, D. Van Gauwbergen, I. Vinckier, pneumatic drying: the use of large-scale experimental data in a design procedure, Powder Technol. 83 (1995) 139–148.
[6] R.D. Radford, A model of particulate drying in pneumatic conveying systems, Powder Technol. 93 (1997) 109–126.
[7] Won Namkung, Minyoung Cho, Pneumatic drying of iron ore particles in a vertical tube, Dry. Technol. 22 (2004) 877–891.
[8] L.A.P. Freitas, J.T. Freire, Gas-to-particle heat transfer in the draft tube of a spouted bed, Dry. Technol. 19 (6) (2001) 1065–1082.
[9] T. Kudra, A.S. Mujumdar, G.S.V. Raghavan, Gas-to-particle heat transfer in two-dimensional spouted beds, Int. Commun. Heat Mass Transfer 16 (1989) 731–741.
[10] A. Raju, V. Sita Rama, J.P. Subrahamanyam, T.R. Rao, B. Pitchumani, Gas–solid heat transfer in cyclone heat exchanger, Indian Chem. Eng., Sect. A 36 (1–2) (1994) 58–62.
[11] N.I. Gelperin, V.G. Einstein, Heat transfer in fluidized beds, in: J.F. Davidson, D. Harrison (Eds.), Fluidization, Academic Press, London, 1971, pp. 517–532.
[12] H.T. Bi, J.R. Grace, J.X. Zhu, On types of choking in pneumatic systems, Int. J. Multiphase Flow 19 (1993) 1077–1092.
[13] J.S. Mei, E.R. Monazam, L.J. Shadle, Flow regime study of a light material in an industrial scale cold flow circulating fluidized bed, J. Energy Resour. Technol. 128 (2006) 129–134.
[14] D.F. King, Estimation of dense bed voidage in fast and slow fluidized beds of FCC catalysts, in: J.R. Grace, L.W. Shemilt, M.A. Bergougnou (Eds.), Fluidization VI, New York, 1989, p. 1.
[15] Jinghai Li, Modeling in advances in chemical engineering, in: M. Kwauk (Ed.), Fast Fluidization, vol. 20, Academic Press, Inc., San Diego, 1994, p. 148.
[16] A.S. Issangya, Flow Dynamics in High Density Circulating Fluidized beds, Ph.D. thesis, The University of British Columbia, Vancouver, Canada, 1998.
[17] S.W. Kim, G. Kirbas, H. Bi, C.J. Lim, Flow behavior and regime transition in a high-density circulating fluidized bed riser, Chem. Eng. Sci. 59 (2004) 3955–3963.
[18] K.S. Rajan, B. Pitchumani, S.N. Srivastava, B. Mohanty, Two-dimensional simulation of gas–solid heat transfer during pneumatic conveying, Int. J. Heat Mass Transfer 50 (5–6) (2007) 967–976.
[19] C.P. Narimatsu, M.C. Ferreira, J.T. Freire, Drying of porous alumina particles in a vertical pneumatic dryer, in: Drying 2004 – Proceedings of the 14th International Drying Symposium (IDS 2004), Sao Paulo, Brazil, 22–25 August 2004, vol. A, pp. 549–556.
[20] L.M. Ludera, Design methods for cyclone preheaters of rotary kilns, Zement Kalk Gips 41 (11) (1988) 551–558 (translation in Zement Kalk Gips 1 (1989) 10–12).